Multi-MeV Electron Acceleration by Subterawatt Laser Pulses

A. J. Goers, G. A. Hine, L. Feder, B. Miao, F. Salehi, J. K. Wahlstrand, and H. M. Milchberg

Institute for Research in Electronics and Applied Physics, University of Maryland, College Park, Maryland 20742, USA

We demonstrate laser-plasma acceleration of high charge electron beams to the ∼10 MeV scale using ultrashort laser pulses with as little energy as 10 mJ. This result is made possible by an extremely dense and thin hydrogen gas jet. Total charge up to ∼0.5 nC is measured for energies >1 MeV. Acceleration is correlated to the presence of a relativistically self-focused laser filament accompanied by an intense coherent broadband light flash, associated with wave breaking, which can radiate more than ∼3% of the laser energy in a ∼1 fs bandwidth consistent with half-cycle optical emission. Our results enable truly portable applications of laser-driven acceleration, such as low dose radiography, ultrafast probing of matter, and isotope production.

Laser-driven electron acceleration in plasmas has achieved many successes in recent years, including record acceleration up to 4 GeV in a low emittance quasimonoenergetic bunch [1] and generation of high energy photons [2–5]. In these experiments, the driver laser pulse typically propagates in the "bubble" or "blowout" regime [6,7] for a normalized peak vector potential $a_0 = eA_0/mc^2 \gg 1$. Plasma densities are deliberately kept low for resonant laser excitation and to avoid dephasing [7]. Essentially all of these experiments use 10 TW −1 PW laser drivers, with repetition rates ranging from 10 Hz to one shot per hour [8].

For many modest lab scale and portable applications, however, a compact, relatively inexpensive, high average current source of laser-accelerated relativistic electrons is sufficient and desirable. In this Letter we describe experiments using a very dense and thin hydrogen gas jet, where the relativistic self-focusing threshold is exceeded even with ∼10 mJ laser pulses and MeV-scale energy electron bunches are generated. This enables applications, such as ultrafast low dose medical radiography, which would benefit from a truly portable source of relativistic charged particle beams. We note that prior work has shown electron bunch generation of modest charge and acceleration (∼10 fC/pulse, <150 keV) from a 1 kHz, ∼10 mJ laser driving a thin (∼100 μm), low density continuous flow argon or helium jet [9].

Central to our experiment is a thin, high density pulsed hydrogen gas jet, which reaches a maximum peak molecular density of 9×10^{20} cm^{-3}, and when fully ionized can exceed the plasma critical density, $N_{cr} = 1.7 \times 10^{21}$ cm^{-3} at our laser central wavelength of $\lambda_0 = 800$ nm. The density profile is near Gaussian, with a full width at half maximum (FWHM) in the range 150–250 μm, depending on the height of the optical axis above the jet orifice. Earlier versions of this jet were run in both pulsed [10] and continuous flow [11] for nitrogen and argon. High densities

are achieved using a combination of high valve backing pressure and cryogenic cooling of the valve feed gas, which is forced through a 100 μm diameter needle orifice. We note that recent laser interaction experiments at near critical density [12] have used a complex pressure-boosted millimeter-scale gas jet [13].

Figure 1 shows the experimental setup. Pulses from a Ti: sapphire laser (50 fs, 10–50 mJ) are focused into the gas jet [Fig. 1(a)] with an $f/9.5$ off-axis paraboloid to a spot size $w_{FWHM} = 8.4$ μm (1.2 × the diffraction limit) containing 80% of the pulse energy, with a confocal parameter of 550 μm. For maximizing electron beam charge and energy, it was found that placing the focused beam waist at the center of the gas jet was optimal, without strong sensitivity to positioning. This is consistent with the laser confocal parameter being more than twice the jet width.

The neutral jet density and plasma profiles were measured using a 400 nm, 70 fs probe pulse [Fig. 1(b), derived from the main pulse] directed perpendicularly through the gas jet to a folded wave front interferometer. Forward- and side-directed optical spectra were collected by fiber-coupled spectrometers, with the forward spectra directed out of the path of the pump laser and electron beam by a pellicle [Fig. 1(c)]. Shadowgraphic images using the 400 nm probe and images of bright broadband wave breaking radiation flashes [Fig. 1(g)] were collected using achromatic optics.

Relativistic electron spectra in the energy range 2–15 MeV were measured using a 0.13 T permanent magnet spectrometer 25 cm downstream of the gas jet [Fig. 1(f)]. A copper plate with a 1.7 mm × 12 mm slit aperture in front of the magnet entrance [Fig. 1(e)] provided energy resolution while allowing measurement of beam divergence in 1D. Electron spectra were dispersed along a LANEX scintillating screen, shielded against exposure to the laser by 100 μm thick aluminum foil, and imaged using a low noise CCD camera. Full electron beam profiles
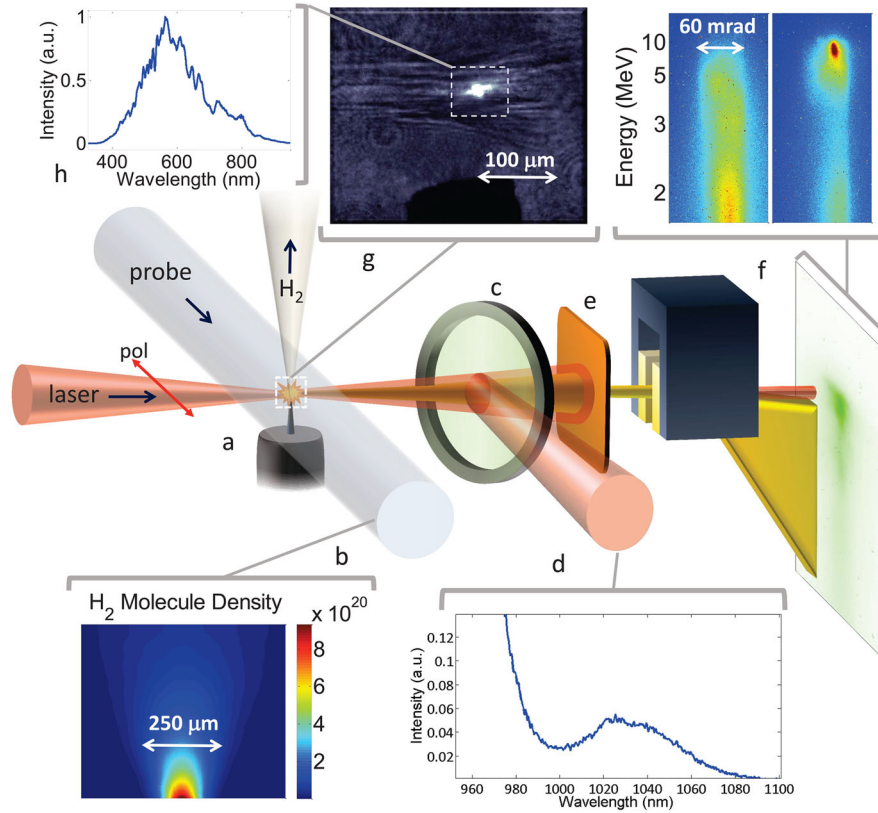
FIG. 1 (color online).   Experimental setup. A horizontally polarized Ti:sapphire laser pulse (10–50 mJ, 50 fs, $\lambda = 800$ nm) interacts with a cryogenically cooled, dense thin H_2 gas jet (a), whose neutral and plasma density profiles are measured by 400 nm probe interferometry (b). A portion of the transmitted laser pulse is reflected by a pellicle (c) and measured by a spectrometer (d). The electron beam from the jet is apertured by a 1.7 mm horizontal slit (e), enters a 0.13 T permanent magnet spectrometer, and is dispersed on an aluminum foil–shielded LANEX screen (f), which is imaged by a low noise CCD camera (not shown). (f) Shows example quasimonoenergetic and exponential spectra for a 40 mJ pulse at $N_e = 2 \times 10^{20}$ cm^{-3}. Shadowgraphic imaging of the laser interaction region above the needle orifice (g) (needle seen as a shadow at bottom) and imaging (g) and spectroscopy (h) of the wave breaking flash. The pump polarization could also be rotated to the vertical by a half wave plate.

were collected on the LANEX screen by translating the dispersing magnets and slit aperture out of the way. Estimates of the accelerated charge were made by calibrating the imaging system and using published LANEX conversion efficiencies [14].

The high density of our target has the immediate effect of enabling relativistic self-focusing of low energy laser pulses leading to the generation of a nonlinear plasma wake. Furthermore, the reduced laser group velocity (and therefore plasma wave phase velocity) at high density drops the threshold for electron injection. Figure 2 shows >1 MeV electron beam generation for pulse energies in the range 10–50 mJ, or 0.2–1.0 TW, as a function of peak plasma density. Beam divergence is $\lesssim 200$ mrad. The results are consistent with the inverse density scaling of the relativistic self-focusing critical power, $P_{\mathrm{cr}} = 17.4(N_{\mathrm{cr}}/N_e)$ GW [15], and the laser power threshold for appearance of a relativistic electron beam is $\sim 3P_{\mathrm{cr}}$ across our range of conditions.

Electron energy spectra in the range 2–12 MeV are shown in Fig. 3(a) for laser pulse energy 10–50 mJ and

peak electron density $N_e = 4.2 \times 10^{20}$ cm^{-3}, with the inset showing total accelerated charge >2 MeV up to ~ 1.2 nC/sr for 50 mJ laser pulses. An electron spectrum simulated from a TurboWAVE 3D particle in cell (PIC)
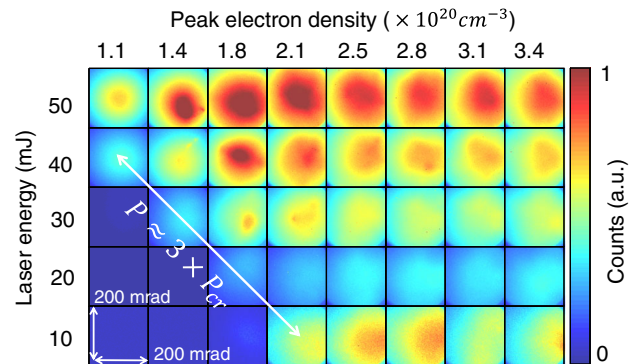

FIG. 2 (color online).   Single shot electron beam images for energies >1 MeV for a range of laser energies and peak electron densities. The color palette was scaled up by $10\times$ for the 10 mJ column. The onset laser power for detectable electron beam generation was $\sim 3P_{\mathrm{cr}}$ across our range of conditions.
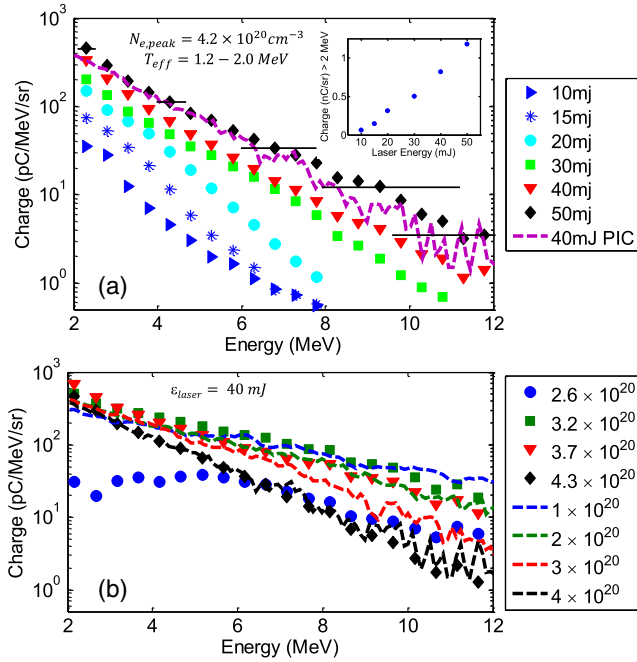
FIG. 3 (color online).   (a) Accelerated electron spectra for peak jet electron density 4.2×10^{20} cm^{-3} for varying laser energy. The inset shows total charge >2 MeV as a function of laser energy. The range of effective temperatures of these exponential-like distributions is indicated. The horizontal black lines indicate the experimental uncertainty in the energy, determined by geometry-limited spectrometer resolution. The dashed curve is a 3D PIC simulation for 40 mJ pump which has been scaled by a factor 0.14 to line up with the experimental curve for 40 mJ. (b) Accelerated electron spectra at laser energy 40 mJ for varying peak electron density. The dashed curves are from 3D PIC simulations and were scaled by the factor 0.14.

simulation [16] for the 40 mJ case is overlaid on the plot. Electron spectra as a function of peak density for fixed pulse energy of 40 mJ are shown in Fig. 3(b) along with results from the 3D PIC simulations. We note that for approximately 20% of shots near the self-focusing onset at each pressure, we observed quasimonoenergetic peaks ranging from 3 MeV (~25 fC for 10 mJ) to 10 MeV [~1.4 pC for 50 mJ, see Fig. 1(f)] with ~10 mrad beam divergence. Both the spectra and the beam spot positions are highly variable and are the subject of ongoing work.

Another consequence of the high density gas target interaction is that the pump pulse envelope is multiple plasma periods long. Over our experimental density range of $N_e = 1$–4×10^{20} cm^{-3}, the plasma period is $2\pi/\omega_p \sim$ 11 fs–5.7 fs, placing our 50 fs pump pulse in the self-modulated laser wakefield acceleration (SM-LWFA) regime. Evidence of SM-LWFA is seen in the moderately collimated electron beams of Fig. 2 and the exponential electron spectra of Fig. 3, reflecting acceleration from strongly curved plasma wave buckets and electron injection into a range of accelerating phases. This is consistent with prior SM-LWFA experiments [17], except that here our dense

hydrogen jet enables production of MeV spectra with laser pulses well below 1 TW. Further confirmation of self-modulation is seen in the spectrum of Raman forward scattered Stokes radiation shown in Fig. 1(d), for the case of laser energy 50 mJ (vacuum $a_0 \sim 0.8$) and peak density $N_e = 1.8 \times 10^{20}$ cm^{-3}. The strong broadband redshifted Raman peak located at $\lambda_s = 2\pi c/\omega_s \sim 1030$ nm enables the estimate of self-focused $a_{SF} \sim 2.7$, using the measured electron density profile and $\omega_s = \omega - \omega_p/\gamma^{1/2}$, where ω is the laser frequency and $\gamma = (1 + a_{SF}^2/2)^{1/2}$ is the relativistic factor. This estimate is in good agreement with the peak a_{SF} in our 3D PIC simulations.

In order for electrons to be accelerated, they must first be injected into the wakefield. Our 3D simulations show catastrophic transverse wave breaking [18] of the strongly curved plasma wave fronts [19] behind the laser pulse, which injects electrons from a wide spread of initial trajectories into a range of phases of the plasma wave. Wave breaking is accompanied by an extremely strong broadband radiation flash emitted by electrons accelerated from rest to near the speed of light in a small fraction of a plasma wavelength. Figure 1(g) shows a magnified single shot image of the sideways-collected flash superimposed on a shadowgram image of the relativistically self-focused filament. Figure 4 shows 10-shot average images of the flash for varying plasma peak density and laser energy collected along the pump polarization direction. Such radiation has been observed in prior work, although at a much lower energy and yield (~0.1 nJ for a 500 mJ pump pulse) [20]. Here, neutral density filters were employed to prevent the side-imaged flash intensity from saturating our CCD. We measure flash energies of ~15 μJ into $f/2.6$ collection optics for the 40 mJ, $N_e = 3.4 \times 10^{20}$ cm^{-3} panel in Fig. 4, giving ~1.5 mJ or >3% of the laser energy if emitted into 4π sr.

The axial location, total energy, and spectrum of the horizontally polarized component of the side-imaged flash are independent of pump polarization, so the flashes do not originate from pump scattering. When the flash is collected perpendicular to the pump polarization, the vertically polarized component has a small contribution at 800 nm, attributed to Thomson scattering, on top of the broadband flash spectrum [21]. Broadband flash spectra (10 shot averages, with no filtering of the pump), peaking at $\lambda_{rad} \sim 550$–600 nm with bandwidth ~400 nm, are shown at the bottom of Fig. 4 for pump energy 40 mJ and a range of densities. The figure panels show that the flash occurs on the hydrogen density profile up-ramp for higher densities and laser energies and on the down-ramp for lower densities and laser energies, as also borne out by our 3D simulations. This is explained by the earlier onset of relativistic self-focusing for higher density or laser energy, which is followed closely by self-modulation and wave breaking.

A question arising in studies of acceleration at higher plasma densities is the relative contributions of laser
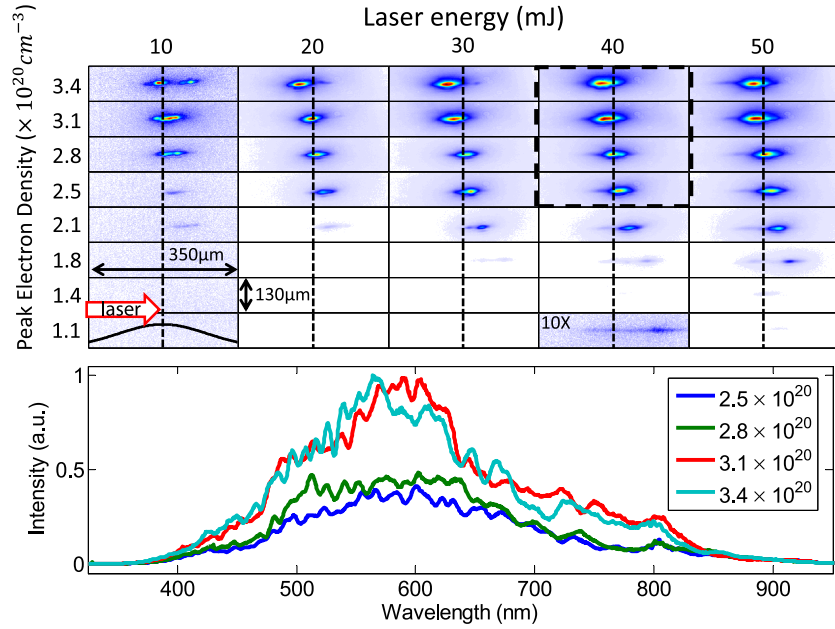
FIG. 4 (color online). *Top panel:* Side images of intense radiation flashes from wave breaking (10 shot averages). The horizontally polarized pump laser pulse propagates left to right. Image intensities are normalized to the maximum intensity within each column. The vertical dashed line is the center of the gas jet, whose profile is shown in the lower left. The 40 mJ, 1.1×10^{20} cm^{-3} image for vertical pump polarization (enhanced 10×), is dominated by 800 nm Thomson scattering on the left and the flash on the right. *Bottom panel:* Spectra (10 shot averages) of the flash for conditions enclosed by the dashed black box in the top panel.

wakefield acceleration (LWFA) and direct laser acceleration (DLA) through resonant betatron oscillation about the wake ion column [22–24]. Early injection on the density profile up-ramp occurs when the plasma wavelength is decreasing and more wake buckets lie under the laser pulse envelope, exposing injected electrons to DLA. On the down-ramp, the plasma wavelength is increasing and fewer buckets lie under the laser field envelope, so that injected electrons are less exposed to the laser field. The flash images of Fig. 4 map injection locations through the jet, and therefore spatially map the relative balance of DLA and LWFA, predicting that DLA dominates at high density (high laser energy) and LWFA dominates at low density (low laser energy). This transition from LWFA to DLA is corroborated by particle tracking in 2D PIC simulations described in [25].

The huge increase in radiation flash energy compared to earlier experiments [20] stems from its coherent emission by electron bunches wave breaking over a spatial scale much smaller than the radiation wavelength and the consequent damping of these bunches by this radiation. As a rough estimate of this effect using 1D approximations, the near-wave-breaking crest width Δx_{crest} of the nonlinear plasma wave is given by $\Delta x_{\text{crest}}/\lambda_p \sim (1/\pi)(\omega/\omega_p)^{3/4}(\Delta p_0/2mc)^{3/4}$ [26], where Δp_0 is the electron initial momentum spread. For $N_e = 3 \times 10^{20}$ cm^{-3} and $\Delta p_0/mc \sim 0.06$ [from an initial spread $\sim (\Delta p_0)^2/2m$ <1 keV from residual electron heating after ionization [27]] we get $\Delta x_{\text{crest}}/\lambda_p \sim 0.04$, or $\Delta x_{\text{crest}} \sim 0.12\lambda_{\text{rad}}$,

significantly shorter than the peak radiated wavelength, ensuring coherent emission. The wave breaking electrons radiate as they execute curved orbits into the wake bucket just ahead of the crest, with emission power $P \sim n^2[(2e^2/3m^2c^3)\gamma^2|d\mathbf{p}/dt|^2]$ [28] and total radiated energy $\varepsilon_{\text{rad}} \sim P\Delta t \sim P\Delta x_{\text{crest}}\gamma^{-1}/c$, where n is the number of accelerating electrons from the crest, $d\mathbf{p}/dt$ is the force on an electron, and Δt is the subfemtosecond time for acceleration off the crest (accounting for Lorentz contraction), or equivalently, the crest lifetime. Taking $n \sim N_e\lambda_p^3$, $\gamma = \gamma_p = \omega/\omega_p$, and $|d\mathbf{p}/dt| \sim eE_{\text{wb}}$, where $E_{\text{wb}} = \sqrt{2}\,(m\omega_p c/e)(\gamma_p - 1)^{1/2}$ is the 1D wave breaking field [18], gives a total radiated energy of $\varepsilon_{\text{rad}} \sim 2$ mJ, which is of the correct order of magnitude.

The strong curving of injected electron orbits by the ion column allows an estimate of the flash spectrum range using the synchrotron radiation critical frequency $\omega_{\text{rad}} \sim \omega_c \sim 3c\gamma^3/2\rho$ [28], where ρ is the orbit radius of curvature, which we take as $\rho \sim \lambda_p$, assuming trapping within a single plasma wave bucket. This gives $\lambda_c \sim 4\pi/3(N_e/N_{\text{cr}})\lambda_0 \sim$ 400–700 nm for the density range shown in Fig. 4, reasonably overlapping the measured spectra. The synchrotron spectrum bandwidth is estimated as $(\Delta\lambda/\lambda)_{\text{rad}} \sim (\omega_{\text{rad}}\Delta t)^{-1} \sim 1$, in accord with the ~ 1 fs bandwidth in Fig. 4 characteristic of half-cycle optical emission, which is consistent with the violent unidirectional electron acceleration upon wave breaking.

To probe its temporal duration and coherence, the flash was interfered in the frequency domain with a

supercontinuum pulse, well-characterized in amplitude and phase, generated in a Xe gas cell [29,30]. Fringes across the full flash spectrum were observed with high visibility, and the spectral phase extracted from the fringes is consistent with the flash being a nearly transform-limited pulse of ~1 fs duration [21]. To our knowledge, this is the first evidence of bright half-cycle optical emission. We note that half-cycle wave breaking radiation at high γ has been proposed as an attosecond x-ray source [31].

In summary, we have demonstrated electron acceleration to the 10 MeV scale with laser pulses well below 1 TW, using a thin, high density hydrogen gas jet, with efficiency of laser energy to MeV electrons of a few percent. The high plasma density reduces the thresholds for relativistic self-focusing, nonlinear plasma wave generation, and electron injection. The reduced spatial scales associated with high density yields intense coherent wave breaking radiation, whose ~1 fs bandwidth is consistent with half-cycle optical emission upon violent unidirectional electron acceleration from rest to nearly the speed of light over a subwavelength distance. The flash is of sufficient intensity to self-damp the injected bunch, with the result that wave breaking radiation and acceleration are comparable energy channels. Our results open the way to applications of relativistic electron beams with truly compact and portable high repetition rate laser systems.

[1] W. P. Leemans et al., Phys. Rev. Lett. **113**, 245002 (2014).

[2] S. Kneip et al., Nat. Phys. **6**, 980 (2010).

[3] S. Cipiccia et al., Nat. Phys. **7**, 867 (2011).

[4] H. Schwoerer, B. Liesfeld, H. P. Schlenvoigt, K. U. Amthor, and R. Sauerbrey, Phys. Rev. Lett. **96**, 014802 (2006); S. Chen et al., Phys. Rev. Lett. **110**, 155003 (2013).

[5] H.-P. Schlenvoigt et al., Nat. Phys. **4**, 130 (2008).

[6] A. Pukhov and J. Meyer-ter-Vehn, Appl. Phys. B **74**, 355 (2002).

[7] W. Lu, M. Tzoufras, C. Joshi, F. S. Tsung, W. B. Mori, J. Vieira, R. A. Fonseca, and L. O. Silva, Phys. Rev. ST Accel. Beams **10**, 061301 (2007).

[8] E. W. Gaul et al., Appl. Opt. **49**, 1676 (2010).

[9] Z.-H. He, B. Hou, J. A. Nees, J. H. Easter, J. Faure, K. Krushelnick, and A. G. R. Thomas, New J. Phys. **15**, 053016 (2013).

[10] A. J. Goers, S. J. Yoon, J. A. Elle, G. A. Hine, and H. M. Milchberg, Appl. Phys. Lett. **104**, 214105 (2014).

[11] D. G. Jang, Y. S. You, H. M. Milchberg, H. Suk, and K. Y. Kim, Appl. Phys. Lett. **105**, 021906 (2014).

[12] F. Sylla, A. Flacco, S. Kahaly, M. Veltcheva, A. Lifschitz, V. Malka, E. d'Humières, I. Andriyash, and V. Tikhonchuk, Phys. Rev. Lett. **110**, 085001 (2013); F. Sylla, A. Flacco, S. Kahaly, M. Veltcheva, A. Lifschitz, G. Sanchez-Arriaga, E. Lefebvre, and V. Malka, Phys. Rev. Lett. **108**, 115003 (2012).

[13] F. Sylla, M. Veltcheva, S. Kahaly, A. Flacco, and V. Malka, Rev. Sci. Instrum. **83**, 033507 (2012).

[14] Y. Glinec, J. Faure, A. Guemnie-Tafo, V. Malka, H. Monard, J. P. Larbre, V. De Waele, J. L. Marignier, and M. Mostafavi, Rev. Sci. Instrum. **77**, 103301 (2006); A. Buck et al., Rev. Sci. Instrum. **81**, 033301 (2010).

[15] G. Schmidt and W. Horton, Comments Plasma Phys. Control. Fusion **9**, 85 (1985); G. Z. Sun, E. Ott, Y. C. Lee, and P. Guzdar, Phys. Fluids **30**, 526 (1987).

[16] D. F. Gordon, IEEE Trans. Plasma Sci. **35**, 1486 (2007).

[17] A. Modena et al., Nature (London) **377**, 606 (1995); D. Umstadter, S.-Y. Chen, A. Maksimchuk, G. Mourou, and R. Wagner, Science **273**, 472 (1996); C. I. Moore, A. Ting, K. Krushelnick, E. Esarey, R. F. Hubbard, B. Hafizi, H. R. Burris, C. Manka, and P. Sprangle, Phys. Rev. Lett. **79**, 3909 (1997).

[18] S. V. Bulanov, F. Pegoraro, A. M. Pukhov, and A. S. Sakharov, Phys. Rev. Lett. **78**, 4205 (1997).

[19] S. V. Bulanov, F. Pegoraro, and A. M. Pukhov, Phys. Rev. Lett. **74**, 710 (1995).

[20] A. G. R. Thomas, S. P. D. Mangles, Z. Najmudin, M. C. Kaluza, C. D. Murphy, and K. Krushelnick, Phys. Rev. Lett. **98**, 054802 (2007).

[21] B. Miao, A. J. Goers, L. Feder, G. A. Hine, F. Salehi, J. K. Wahlstrand, D. Woodbury, and H. M. Milchberg (to be published).

[22] A. Pukhov, Z.-M. Sheng, and J. Meyer-ter-Vehn, Phys. Plasmas **6**, 2847 (1999).

[23] C. Gahn, G. D. Tsakiris, A. Pukhov, J. Meyer-ter-Vehn, G. Pretzler, P. Thirolf, D. Habs, and K. J. Witte, Phys. Rev. Lett. **83**, 4772 (1999).

[24] J. L. Shaw, F. S. Tsung, N. Vafaei-Najafabadi, K. A. Marsh, N. Lemos, W. B. Mori, and C. Joshi, Plasma Phys. Controlled Fusion **56**, 084006 (2014).

[25] Supplemental Material at http://link.aps.org/supplemental/10.1103/PhysRevLett.115.194802 for description of PIC simulation and results.

[26] S. V. Bulanov et al., Phys. Plasmas **19**, 113102 (2012).

[27] B. M. Penetrante and J. N. Bardsley, Phys. Rev. A **43**, 3100 (1991).

[28] J. D. Jackson, Classical Electrodynamics, 3rd ed. (Wiley, New York, 2001).

[29] Y.-H. Chen, S. Varma, A. York, and H. M. Milchberg, Opt. Express **15**, 11341 (2007).

[30] K. Y. Kim, I. Alexeev, and H. M. Milchberg, Appl. Phys. Lett. **81**, 4124 (2002).

[31] F. Y. Li, Z. M. Sheng, M. Chen, L. L. Yu, J. Meyer-ter-Vehn, W. B. Mori, and J. Zhang, Phys. Rev. E **90**, 043104 (2014).